

1
2
3
4
5
6
7
8
9
10
11
12
13
14
15
16
17
18
19
20
21
22
23
24
25

Alterations on growth and cell organization of *Giardia intestinalis* trophozoites after treatment with KH-TFMDI, a novel class III histone deacetylase inhibitor

Ana Paula R. Gadelha^a, Bárbara Bravim^a, Juliana Vidal^b, Lissa Catherine Reignault^b, Bruno Cosme^a, Kilian Huber^{c, d}, Franz Bracher^c, Wanderley de Souza^{a, b, e, *}

^a*Diretoria de Metrologia Aplicada a Ciências da Vida, Instituto Nacional de Metrologia, Qualidade e Tecnologia, Rio de Janeiro, RJ, Brazil*

^b*Instituto de Biofísica Carlos Chagas Filho, Universidade Federal do Rio de Janeiro, Rio de Janeiro, RJ, Brazil*

^c*Department of Pharmacy, Center for Drug Research, Ludwig-Maximilians-University of Munich, Munich, Germany*

^d*Nuffield Department of Medicine, University of Oxford, Oxford, UK*

^e*Instituto Nacional de Ciência e Tecnologia em Biologia Estrutural e Bioimagens e Centro Nacional de Biologia Estrutural e Bioimagens, Universidade Federal do Rio de Janeiro, Rio de Janeiro, RJ, Brazil*

*** Corresponding author:**

Wanderley de Souza. Laboratório de Ultraestrutura Celular Hertha Meyer, Instituto de Biofísica Carlos Chagas Filho, Universidade Federal do Rio de Janeiro, Avenida Carlos Chagas Filho, 373, CCS, Bloco G-subsolo, Cidade Universitária, 21941-902 Rio de Janeiro, RJ, Brazil. Tel/Fax: +55 21; Fax: +55 21 2260 2364.

E-mail address: wsouza@biof.ufrj.br

27 **ABSTRACT**

28 *Giardia* trophozoites have developed resistance mechanisms to currently available
29 compounds, leading to treatment failures. In this context, the development of new additional agents
30 is mandatory. Sirtuins, which are class III NAD⁺-dependent histone deacetylases, have been
31 considered important targets for the development of new anti-parasitic drugs. Here, we evaluated
32 the activity of KH-TFMDI, a novel 3-arylideneindolin-2-one-type sirtuin inhibitor, on *G.*
33 *intestinalis* trophozoites. This compound decreased the trophozoite growth presenting an IC₅₀ value
34 lower than nicotinamide, a moderately active inhibitor of yeast and human sirtuins. Light and
35 electron microscopy analysis showed the presence of multinucleated cell clusters suggesting that the
36 cytokinesis could be compromised in treated trophozoites. Cell rounding, concomitantly with the
37 folding of the ventro-lateral flange and flagella internalization, was also observed. These cells
38 eventually died by a mechanism which lead to DNA/nuclear damage, formation of multi-lamellar
39 bodies and annexin V binding on the parasite surface. Taken together, these data show that KH-
40 TFMDI has significant effects against *G. intestinalis* trophozoites proliferation and structural
41 organization and suggest that histone deacetylation pathway should be explored on this protozoon
42 as target for chemotherapy.

43

44

45

46

47 **Keywords:** *Giardia intestinalis*, class III NAD⁺-dependent histone deacetylases inhibitor,
48 automated quantitative fluorescence microscopy, electron microscopy, proliferation, cell death.

1. Introduction

Giardia intestinalis is a flagellated protozoan and the causative agent of giardiasis, a disease characterized by symptoms such as chronic diarrhea, nausea and a stomach cramps (Buret, 2008). *Giardia* is a waterborne parasitic protozoan with a worldwide distribution (Karanis et al., 2007). Current giardiasis treatment is based on 5-nitroimidazole compounds, of which metronidazole is the most commonly used drug in many countries. This compound is activated in *G. intestinalis* when the 5-nitro group is reduced by oxidoreductase enzymes (Gardner and Hill, 2001; Emery et al., 2018) and the toxic metabolites formed by reduction can interact with several cell structures and molecular targets (Campanati and Monteiro-Leal, 2002; Oxberry et al., 1994; Uzlikova et al., 2014). Other compounds used to treat giardiasis are benzimidazole derivatives, such as albendazole, which bind to tubulin (MacDonald et al., 2004), inhibiting *Giardia* growth and changing cytoskeletal elements (Morgan et al., 1993; Pérez-Rangel et al., 2013). Metronidazole and albendazole were first developed to treat other parasitic infections, and introduced for giardiasis treatment about five decades ago. Although these drugs are still used against giardiasis, treatment failures and parasite resistance emerged over the decades (Argüello-García et al., 2009; Tejman-Yarden and Eckmann, 2011). Therefore, because of the prevalence of the disease, the development of new therapeutic agents is mandatory.

Histone acetylation is controlled by the activity of histone acetyltransferases (HATs), which contribute to chromatin decondensation and activation of transcription, and histone deacetylases (HDACs), which promote chromatin condensation and gene silencing (Kouzarides, 2007). In mammalian cells, HDACs are grouped into different classes, consisting of the ubiquitously expressed class I (HDACs 1–3, 8), the tissue-specific classes II (HDACs 4–7, 9, 10) and IV (HDAC11), and class III, composed of seven sirtuins (SIRT1–7). Sirtuins cleave the acetyl groups from lysine residues in histones and other proteins in a unique manner, since they are not zinc-dependent, but require nicotinamide adenine dinucleotide (NAD⁺) as a co-factor for catalysis

76 (Abend and Kehat, 2015). Sirtuins target different acetylated protein substrates and are localized to
77 distinct cell compartments. They modulate numerous cellular processes, including the cell cycle,
78 microtubule organization, mitochondrial activity, DNA repair, and cell death (Horio et al., 2011;
79 Inoue et al., 2007; Verdin et al., 2010). Sirtuins have also been found in various parasitic protozoa,
80 including *Plasmodium falciparum*, where they were associated with antigenic variation regulation
81 (Merrick et al., 2015). In the trypanosomatid parasites *Trypanosoma cruzi* (Ritagliati et al., 2015)
82 and *Trypanosoma brucei* (Alsford et al., 2007), sirtuin activity was important for the proliferation of
83 replicative forms, the host cell-parasite interaction, cell differentiation, and DNA repair. Sirtuin
84 expression was also detected in *Leishmania* (Vergnes et al., 2005; Zemzoumi et al., 1998), in which
85 Sir2-related proteins were involved in the control of survival and cell death. The analysis of *G.*
86 *intestinalis* genome showed the presence of five sirtuin type 2 family homologues:
87 GL50803_10708, GL50803_10707, GL50803_11676, GL50803_6942 and GL50803_16569
88 (Sonda et al., 2010; Giardia DB: <http://giardiadb.org>). As pointed out by Carranza et al. (2016),
89 three *Giardia* sirtuins (GL50803_10707; GL50803_10708; GL50803_11676) may be
90 phylogenetically classified as belonging to class I, whereas other two sirtuins are more closely to
91 class III Sirt5 from human (GL50803_16569) and subclass U of bacterial sirtuins (GL50803_6942)
92 (Religa and Waters, 2012; Wang et al., 2016). *Giardia* sirtuins are localized in the trophozoite
93 nucleus, with exception of GL50803_10708, which has cytoplasmic localization and may not be
94 related to genetic regulation (Carranza et al., 2016).

95 In view of the biological role played by HDAC, classic inhibitors of class III histone
96 deacetylases have been commercially available and have become interesting alternatives for the
97 treatment of neoplastic and age-associated diseases and other pathologies (Carafa et al., 2012).
98 Sirtinol, a commercially available SIRT2 inhibitor, was investigated for its activity against
99 *Leishmania infantum* and inhibited amastigote multiplication and promoted cell death associated
100 with DNA fragmentation (Vergnes et al., 2005). Nicotinamide, a moderately active inhibitor of
101 yeast and human sirtuins, was able to inhibit *Plasmodium falciparum* and *Trypanosoma cruzi*

102 proliferation (Prusty et al., 2008; Soares et al., 2012) and *Giardia* encystation process (Carranza et
103 al., 2016). When used against *T. cruzi* and *L. amazonensis*, KH-TFMDI, a novel 3-arylideneindolin-
104 2-one-type inhibitor of NAD⁺ dependent histone deacetylases (Huber et al., 2010), caused growth
105 arrest and induced programmed cell death (Veiga-Santos et al., 2014; Verçoza et al., 2017). In view
106 of these observations we decided to investigate the activity of KH-TFMDI on *G. intestinalis*
107 trophozoites. The human sirtuins have three active pocket sites, A, B and C; the last one is proposed
108 to have a regulatory role (Avalos et al., 2005). KH-TFMDI has similar activity to cambinol and
109 nicotinamide, at least it shares the specific protein binding site in the C subpocket of the sirtuin 2
110 protein sequence (Avalos et al., 2005; Huber et al., 2010). The NAD⁺ binding site (C subpocket) is
111 highly conserved from protozoan taxa to human, suggesting that KH-TFMDI may have similar
112 activity on different organisms. In the present study, we report that KH-TFMDI inhibits the
113 proliferation of the *G. intestinalis* trophozoites and compromises cytokinesis. This compound also
114 induces several ultrastructure changes. Despite that, these cells eventually die by a process
115 characterized by DNA/nuclear damage, formation of the multi-lamellar bodies and annexin V
116 binding on the cell surface. These results indicate that KH-TFMDI has noteworthy effects against
117 *G. intestinalis*, suggesting that class III NAD⁺-dependent histone deacetylases are potential targets
118 for development of new drugs to treat giardiasis in the future.

120 2. Methods

121

122 2.1. Sirtuin Inhibitor

123 The sirtuin inhibitor KH-TFMDI was synthesized by Huber and Bracher (Huber et al., 2010)
124 at the Department of Pharmacy, Center for Drug Research, Ludwig-Maximilians-University in
125 Munich, Germany. The structure of this compound can be seen in the Supplementary material 1.
126 KH-TFMDI is a member of the 3-arylideneindolin-2-one family, which was previously synthesized
127 to inhibit the human class III NAD⁺-dependent histone deacetylases I and II (Huber et al., 2010;
128 Ong et al., 2017). Stock solutions of the compound (10 mM) were prepared in dimethyl sulfoxide
129 (DMSO) (Merck, Darmstadt, Germany) and stored at -20°C. Metronidazole (Sigma Chemical
130 Company, St. Louis, USA), used as a positive control, was dissolved in sterile water. Nicotinamide
131 (Merck, Darmstadt, Germany), an inhibitor of *Giardia*, yeast and human sirtuins, was dissolved in
132 sterile water at stock concentration of 1 M.

133

134 2.2. Parasites

135 Cultures of *Giardia intestinalis* trophozoites from the WB isolate (ATCC 30957, USA) were
136 grown in 16-ml screw-cap glass culture tubes containing modified TYI-S-33 medium (pH 7.2)
137 enriched with 0.1% bovine bile and 10% fetal bovine serum at 37°C, for 48 to 72 h, as described by
138 Keister (1983).

139

140 2.3. Intestinal epithelial cell cultures

141 Monolayers of human colon epithelial cells (Caco-2 line, ATCC HTB-37, USA) were grown
142 in high-glucose Dulbecco's modified Eagle's medium (DMEM) with 10% fetal bovine serum (FBS)
143 in an atmosphere of 5% CO₂ at 37 °C.

145 2.4. *G. intestinalis* proliferation assays

146 Trophozoites (1×10^5 cells/ml) were inoculated in fresh TYI-S-33 medium in the presence
147 of 1, 5, 10, or 25 μM of KH-TFMDI. The maximum concentration of DMSO was lower than or
148 equal to 0.5%, a concentration that does not interfere with *Giardia* growth (Campanati et al., 1999).
149 Metronidazole was used as positive control at the concentration of 1, 5, 10, or 25 μM . Parasites
150 were also exposed to 1, 10, 20 and 50 mM of nicotinamide. Following growth at 24 and 48 h,
151 untreated and DMSO- or treated parasites were placed on ice for 15 min, cells were diluted 1:10 on
152 4% formaldehyde and counted using a hemocytometer (Neubauer chamber). For all drugs, the
153 concentration that caused a 50% reduction in the reproduction of trophozoites (IC_{50}) was calculated
154 using a dose response curve (log inhibitor vs response) from Prism 6 software
155 (<https://www.graphpad.com>). All experiments were performed at least four times.

156

157 2.5. Mammalian cell cytotoxicity assays

158 Caco-2 cells were trypsinized and 1×10^4 cells/ml were inoculated in 96-well tissue culture
159 plates. After 24 h, KH-TFMDI, at concentrations of 50 or 100 μM , was added to the culture
160 medium and the plates were incubated at 37 °C in 5% CO_2 for 48 h. The final concentration of
161 DMSO was lower than or equal to 1%. Following incubation with these compounds, cells were
162 incubated with Hoechst 33342 (Molecular Probes, USA; 5 $\mu\text{g/ml}$) to identify nuclei. For
163 quantification of the proliferation, live cells were imaged using the IN Cell Analyzer 2000
164 automated cell imaging system (GE Healthcare, UK). The Hoechst signal was detected with
165 excitation 350/50 nm and emission 455/50 nm filters. Ten image fields ($20\times$ objective, image area
166 $0,150 \text{ mm}^2/\text{field}$) were acquired per well, each with an exposure time of 200 ms. The Multi Target
167 Analysis module for IN Cell Analyzer 3.7.2 was used to define and quantify the objects of interest.
168 Nuclear segmentation was chosen to identify Caco-2 cells with a minimum nuclear area of $80 \mu\text{m}^2$
169 and sensitivity level of 80.

170

171 2.6. *Live cell imaging*

172 For live cell imaging, a drop of cell suspension in culture medium was placed onto a slide
173 and gently covered with a coverslip. Control and treated samples were examined with a Zeiss
174 AxioImager light microscope using differential interference contrast (DIC) and a 100× objective
175 under ambient conditions. Images were collected with an Axiocam MRc5 camera driven by
176 AxiVision software. Images were processed using Adobe Photoshop software.

177

178 2.7. *Field emission scanning electron microscopy (FESEM)*

179 Control and treated cultures were fixed for 1 h in a solution containing 2.5% glutaraldehyde
180 in 0.1 M cacodylate buffer (pH 7.2) and post-fixed for 1 h with 1% osmium tetroxide (OsO₄) in 0.1
181 M cacodylate buffer. Cells were dehydrated in an ethanol series, critical point dried in a Leica EM
182 CPD 030 apparatus using CO₂, and ion-sputtered with a platinum layer. Samples were observed in
183 a FEI Quanta FEG 450 field emission scanning electron microscope.

184

185 2.8. *Immunofluorescence microscopy*

186 *Giardia* trophozoites were chilled on ice for 15 min to detach the cells, which were collected
187 by centrifugation (10 min, 1500 g), washed twice with PBS, and then allowed to adhere to
188 previously poly-L-lysine-coated coverslips. After 3 min, the cells were fixed with 1% formaldehyde
189 in PHEM buffer for 1 h. Next, cells were permeabilized with 0.5% Triton X-100 in the same buffer
190 for 10 min, followed by a 1-h blocking step (PBS containing 3% bovine serum albumin (BSA), pH
191 8.0). The cells were then incubated in the presence of the primary antibody TAT-1 kindly provided
192 by Dr. K. Gull (Kohl et al., 1999). After primary antibody incubation, the samples were washed
193 four times with PBS+BSA and incubated for 1 h with the secondary antibody goat anti-mouse IgG
194 coupled to Alexa 546, diluted 1:400 (Molecular Probes, USA). Cells were washed 3 times and
195 incubated with Hoechst stain (Molecular Probes, USA; 5 µg/ml) for 10 min. As a control, the

196 primary antibody was omitted from some samples. Slides were mounted using n-propyl gallate to
197 reduce photobleaching, and fluorescence images were obtained using a Leica TCS SP5 confocal
198 microscope with corresponding beam splitter and barrier filters for imaging.

199

200 2.9. Automated quantitative fluorescence microscopy

201 The samples were assayed as described for the immunofluorescence assay. Briefly, slides
202 were imaged in the IN Cell Analyzer 2000 automated cell imaging system (GE Healthcare, UK).
203 The Hoechst signal was detected with excitation 350/50 nm and emission 455/50 nm filters; the
204 TAT-1 signal was detected with excitation 543/22 nm and emission 605/64 nm filters. Fifty image
205 fields (100× objective, image area 0.006 mm²/field) were acquired per coverslip, each with an
206 exposure time of 500 ms. The IN Cell Developer Toolbox 1.9.2 was used to define and quantify the
207 objects of interest. Nuclear segmentation was chosen to identify trophozoites with a minimum
208 nuclear area of 0.70 μm² and sensitivity level of 92. Typically, a *G. intestinalis* nucleus measured
209 1–2 μm². A post-segmentation processing step was incorporated to eliminate segmentation areas
210 that were less than 8 μm² with kernel size 3. The analyzed parameters were: nuclear area, nuclear
211 intensity, cell area and tubulin labeling intensity.

212

213 2.10. Western blot analysis

214 Trophozoites were harvested, washed twice and resuspended in PBS containing protease
215 inhibitors cocktail (Sigma, USA). Then, the cells were lysed with ten cycles of freezing and
216 thawing. The total cell lysates were mixed with a solution containing 62 mM Tris-HCl, 7%
217 glycerol, 2.5% SDS, 5% β-mercaptoethanol, 0.01% bromophenol blue and boiled for 5 min. Protein
218 concentration was determined by using a Bio-Rad protein assay (Bio-Rad, USA). The lysates at the
219 protein concentration of 35 μg were loading on 7.5% SDS-PAGE. After electrophoresis, proteins
220 were transferred to nitrocellulose membranes, blocked with 5% non-fat milk for 1 h at room
221 temperature and incubated for 2 h with anti-α-tubulin TAT-1 and anti-acetylated tubulin 6-11B-1

222 (Sigma, USA) antibody at 1:10 dilution. Then, the membranes was washed three times and
223 incubated for 1 h with peroxidase-conjugated goat anti-mouse secondary antibody (Promega, USA).
224 Membranes were washed as previously described and visualized using chemiluminescent substrate.

225

226 2.11. Transmission electron microscopy (TEM)

227 For transmission electron microscopy, specimens were fixed for 1 h at room temperature in
228 a solution containing 2.5% glutaraldehyde and 4% formaldehyde in PHEM buffer (pH 7.2).
229 Samples were then washed twice in PBS, pH 7.2, and post-fixed in 1% OsO₄ supplemented with
230 0.8% potassium ferricyanide. Cells were then dehydrated in an acetone series, embedded in Epoxide
231 resin and sectioned in a Reichert ultramicrotome. Ultrathin sections were collected in copper grids
232 and stained with 5% aqueous uranyl acetate and lead citrate, and observed in a FEI Tecnai Spirit
233 transmission electron microscope.

234

235 2.12. Annexin-V and propidium iodide analysis

236 This experiment was performed using a Dead Cell Apoptosis Kit with Annexin V-Alexa
237 Fluor® 488 & Propidium Iodide (Molecular Probes, USA), following the manufacturer's protocol.
238 Briefly, treated and untreated trophozoites were washed with chilled PBS and resuspended in 500 µl
239 of 1× binding buffer. Cells were then incubated with Annexin V-Alexa 488 and propidium iodide
240 for 5 min in the dark at room temperature. Data were collected on a BD FACSCalibur instrument
241 controlled by CellQuest Pro software (BD Biosciences, CA, USA) and analyzed with Summit 4.3
242 (Dako, Fort Collins, CO, USA). A total of 10,000 events were acquired in the regions previously
243 established as those corresponding to *G. intestinalis*. Alternatively, cells incubated with Annexin V-
244 Alexa 488 and propidium iodide were analyzed by immunofluorescence using a Leica DMI600 B
245 fluorescence microscope.

246 2.13. DNA fragmentation analysis

247 Total cellular DNA from treated and untreated cells was isolated and analyzed by
248 acrylamide gel electrophoresis. Briefly, cells were mixed with a lysis buffer (100 mM Tris-HCl, 2
249 mM EDTA, 400 mM NaCl, 2% SDS, pH 8.0) containing 300 µg/ml of proteinase-K in a 56 °C
250 water-bath for 90 min. Samples were centrifuged immediately at 7000 × g for 10 min at 4 °C and
251 the supernatant was washed by adding 800 µl of 100% ethanol and centrifuged at 7000 × g for 10
252 min at 4°C. After, the supernatant was decanted and the DNA pellet was washed by adding 800 µl
253 of 100% ethanol and centrifuged at 7000 × g for 10 min at 4 °C. The resulting pellet was washed by
254 adding 800 µl of 70% ethanol and centrifuged at 7000 × g for 12 min at 4 °C. The pellet was air-
255 dried and resuspended in TE buffer, pH 7.5 (10 mM Tris-Cl, 0.1 mM of pH 8.0 EDTA). Total DNA
256 was mixed with a tracking dye present in the sample buffer and loaded on a 7% acrylamide gel.
257 Gels were run for 1 h at 165 V, stained with ethidium bromide, and analyzed using a UV
258 transilluminator (Bio-Rad, USA).

259

260 2.14. Cell cycle analysis

261 Cells growth in 1.5 ml eppendorf tubes (approx. 10⁵ cells in total) were chilled on ice for 20
262 min and collected by centrifugation (5 min; 1500 g; 4° C). Afterward, the medium was replaced, and
263 the cells were fixed with ice cold 70% ethanol. The samples were then centrifuged, washed and
264 resuspended in 500 µl of PBS containing 2.5 µl of RNase A corresponding to 50 µg/ml and
265 incubated for 30 min at 37 °C. Then, the cells were centrifuged and resuspended in 500 µl of PBS
266 containing propidium iodide at a final concentration of 2 µg/ml (Sigma, USA). The analysis was
267 performed using an Accuri C6 cytometer (Becton Dickision, USA). Fifty thousand events were
268 evaluated and the data plotted as cell percentage x cell cycle stage.

269

270 2.15. Multiple sequence alignments

271 Different organisms protein sequences of sirtuins were acquire from NCBI
272 (<http://www.ncbi.nlm.nih.gov/>): *Xenopus leavis* (NP_001088636), *Homo sapiens* SIRT1

273 (NP_036370.2) and SIRT2 (AAK51133.1), *Drosophila melanogaster* (AHN57421.1), *Giardia*
274 *intestinalis* (EET01632), *Trypanosoma grayi* (KEG11227.1), *Leishmania infantum* (AF487351.1),
275 *Entamoeba histolytica* (EHI5A_061340) and *Entamoeba invadens* (EIN_219010). The aminoacid
276 multiple sequence alignments were performed with ClustalW v2.1 under BLOSUM62 score matrix
277 to score pairs of aligned residues.

278

279 2.16. Statistical analysis

280 Values are expressed as mean \pm standard error of the mean, and were compared by two-way
281 ANOVA with a Bonferroni multiple comparison test or one-way ANOVA with Dunnet's multiple
282 comparison test (Prism 6 Software Inc.), as appropriate. *P* values lower than 0.05 were considered
283 statistically significant.

285 3. Results

286

287 3.1. Multiple sequence alignments

288 We performed a multiple sequence alignments of *Giardia* NAD-dependent histone
289 deacetylase Sir2 (GL50803_10707) with the canonical fold of the sirtuins from several organisms
290 (Supplementary material 2). These data showed a high level of similarity between *Giardia* NAD-
291 dependent histone deacetylase Sir2 (GL50803_10707) and the orthologues of other protozoan and
292 metazoan species (Supplementary material 2). The site of zinc ion and NAD⁺ binding (C subpocket
293 binding site), important catalytic domains, were conserved throughout the taxons compared
294 (Supplementary material 2).

295 3.2. KH-TFMDI effects on parasite growth

296 In order to verify the activity of the sirtuin inhibitor KH-TFMDI on *G. intestinalis*
297 proliferation, trophozoites were incubated with different concentrations of the compound for 24 and
298 48 h. The addition of KH-TFMDI led to dose- and time-dependent growth inhibition as shown in
299 Figure 1a. This compound significantly decreased the parasite replication ($p < 0.001$), presenting an
300 IC₅₀ value in the single digit μ M range at 48 h of treatment. Incubation with 10 and 25 μ M KH-
301 TFMDI reduced around 80% cell growth. The concentration of DMSO equivalent to those used in
302 treated cells (i.e., up to 0.5%) did not affect parasite proliferation (Fig. 1a). Metronidazole, the
303 reference drug used as a positive control, reduced parasite replication exhibiting an IC₅₀ value in the
304 single digit μ M range (Fig. 1b). Nicotinamide was also tested and inhibited trophozoite growth
305 presenting an IC₅₀ value in the mM range (Supplementary material 3).

306

307 3.3. Cytotoxicity of KH-TFMDI on mammalian cell viability

308 During infection *Giardia* trophozoites attach and colonize the intestinal epithelium. To
309 analyze the cytotoxicity effects on the mammalian host cells, Caco-2 intestinal cell line was treated
310 for 48 h with 50 or 100 μ M KH-TFMDI (i.e., 50- and 100-fold higher than the IC₅₀ obtained for *G.*

311 *intestinalis* trophozoites). As shown in Supplementary material 4, KH-TFMDI or metronidazole did
312 not alter the intestinal cells proliferation ($p > 0.05$).

313

314 3.4. KH-TFMDI effects on parasite morphology

315 As the concentration of 25 μ M KH-TFMDI caused severe effects on cell growth, it was not
316 included in the subsequent morphological and biochemical assays. Then, to investigate the primary
317 effects of KH-TFMDI on cell structure, parasites were observed after exposure to lower
318 concentrations. Live cell imaging observations showed that untreated cells presented the
319 characteristic pyriform shape with the flagella and two nuclei (Fig. 2a). After exposure to 1 or 5 μ M
320 of KH-TFMDI, trophozoites presented a ruffled surface (Fig. 2b) and rounded appearance (Fig. 2c).
321 Cell division was asymmetric after treatment with this inhibitor (Fig. 2d). Analysis by FESEM of
322 fixed cells confirmed the morphological changes showed by light microscopy. When compared to
323 control trophozoites (Fig. 3a), the parasites treated with 1 or 5 μ M exhibited blebbing on their
324 dorsal surface (Fig. 3b). Cell rounding was observed concomitantly with the folding of the ventro-
325 lateral flange (Fig. 3c) in 31% of the population. KH-TFMDI treatment altered flagella number of
326 22% of the parasites and a large bulbous structure in the flagellar tip could be observed (Fig. 3d). In
327 addition, the formation of large cellular masses was also visualized (15% of cells) mainly after
328 incubation with 10 μ M (Fig. 3e-f).

329

330 3.5. Nuclei and Cytoskeleton organization after KH-TFMDI exposure

331 To better visualize the changes of the cell body and determine the distribution of the
332 cytoskeletal elements, trophozoites were analyzed using DIC microscopy associated with
333 immunofluorescence using the anti- α tubulin antibody TAT-1 and Hoechst stain to label the nuclei.
334 In control cells, tubulin was observed in the flagella, median body, and cytoplasm (Figs. 4a, 4a'').
335 The two nuclei of trophozoites were localized in the anterior region and presented an oval aspect
336 (Figs. 4a'- 4a''). As observed in live cell imaging and FESEM assay, the pyriform shape of

337 trophozoites slightly changed to a rounded aspect after treatment with 1 or 5 μ M KH-TFMDI (Figs.
338 4b, 4b''). Different sizes of Hoechst-stained structures were observed in treated cells (Fig. 4b').
339 After exposure to KH-TFMDI cell cluster were seen with completed karyokinesis (Figs. 4c-4c'').

340 To quantify the morphological changes in the cell body and nucleus of the trophozoites
341 exposed to KH-TFMDI, morphometric analysis were carried out using automated quantitative
342 fluorescence microscopy. This methodology consists in the sequential acquisition of fluorescent
343 images, identification and segmentation of the cell structures and data analysis (quantification,
344 measurement) by automated algorithms included in IN Cell Investigator software. For this, the
345 parasite nuclei and cell body segmentation were based on Hoechst nuclear staining and α -tubulin
346 labeling, respectively (Fig. 5a-b). Morphometric analysis of parasite exposed to KH-TFMDI
347 showed that the nuclear area and labeling intensity (Hoechst stain) increased 25% and 11% on
348 treated parasites ($p < 0.05$) (Fig. 5c-d). Whereas the cell body area increased 45% when compared
349 to control cells (Fig. 5e). This analysis also revealed that treated parasites increased up to 32% the
350 α -tubulin labeling intensity (cell intensity) ($p < 0.05$) (Fig. 5f).

351 To investigate if KH-TFMDI could induce cytoskeleton changes associated to tubulin
352 alterations, we carried out a Western blot analysis using anti- α -tubulin TAT-1 and anti-acetylated
353 tubulin 6-11B-1 antibodies (Fig. 6a-b). The densitometry analysis indicated that there were no
354 modifications in the amount of α -tubulin after treatment (Fig. 6c). The acetylated tubulin expression
355 was slightly decreased within 48 h of addition of 5 μ M KH-TFMDI, however this reduction was not
356 significant (Fig. 6d). Immunofluorescence microscopy images and automated quantitative
357 fluorescence microscopy showed that acetylated tubulin labeling pattern was similar in control and
358 treated cells (Fig. 6e-f).

359

360 3.6. KH-TFMDI effects on parasite ultrastructure

361 Observations of longitudinal sections by TEM showed that untreated cells presented all the
362 characteristic features of normal trophozoites: two round nuclei, intact adhesive disks, flagella

363 axonemes, peripheral vesicles, and a homogeneous cytoplasm filled with ribosomes and glycogen
364 particles (Fig. 7a). In contrast, incubation of the parasite with 1 to 10 μ M KH-TFMDI led to an
365 abnormal distribution of the cytoplasmic content, with areas lacking glycogen particles and
366 ribosomes (Fig. 7b). Asymmetric cell shape profiles were also observed after exposure to the drug
367 (Fig. 7c), as were cytoplasmic vacuolization and axoneme dislocation from characteristic locations
368 (Fig. 7d). Although the structure of the cytoskeleton (adhesive disc, median body, flagella) has not
369 been altered, some flagella were seen internalized (Fig. 7c). Multi-lamellar bodies, which contained
370 cytoplasmic granules, were detected in the trophozoites (Figs. 7e-f). In some analysis, they were
371 seen near dorsal surface and appeared to force the membrane, causing a protrusion (Fig. 7f).
372 Ultrastructure changes were also observed in the nuclei that exhibited polymorphic aspects (Figs.
373 8a-b) and condensed chromatin (Fig. 8c) after incubation with KH-TFMDI.

374

375 3.7. Evaluation of annexin V binding on trophozoites

376 Flow cytometry analyses were carried out to determine if KH-TFMDI could induce early
377 membrane events indicative of cell death in *G. intestinalis* trophozoites. Cells incubated with 1 and
378 10 μ M KH-TFMDI for 48 hours were incubated in the presence of annexin V (a marker for early
379 apoptosis) and propidium iodide (PI) (a marker for membrane damage, possibly late
380 apoptosis/necrosis). Our results revealed that the percentage of labeling with annexin V for control
381 cells was 1% of trophozoites, while the number of PI-positive parasites was 9% (Fig. 9a). In
382 cultures exposure to KH-TFMDI, the levels of annexin V staining were about 50%, whilst levels of
383 PI staining were around 1% (Figs. 9b-c). The annexin V labeling on parasite exposure to KH-
384 TFMDI was confirmed by immunofluorescence microscopy images (Supplementary material 5).

385

386

387

388

389 3.8. *Analysis of DNA damage induced by KH-TFMDI treatment*

390 The effect of the KH-TFMDI on *Giardia* DNA was also examined. When genomic DNA
391 was isolated from trophozoites, sheared fragmented DNA mainly in lower molecular weight regions
392 was detected in cells incubated with KH-TFMDI (Fig. 9d).

393

394 3.9. *Cell cycle analysis*

395 To determine the effects of KH-TFMDI on parasite division, cell cycle progression was
396 followed by analysis of DNA content in control and treated cells by flow cytometer. It was
397 observed a slightly increased (about 10%) in the percentage of cells in G0/G1 and S phase within 48
398 h of addition of 5 μ M KH-TFMDI (Fig. 10).

399

401 **4. Discussion**

402

403 Our observations indicated that KH-TFMDI, a novel inhibitor of NAD⁺ dependent histone
404 deacetylases, significantly reduced the trophozoites proliferation. The *G. intestinalis* growth
405 inhibition was similar to that found for *T. cruzi* (Veiga-Santos et al., 2014) and *L. amazonensis*
406 (Verçoza et al., 2017) after exposure to this compound. The proliferation of *G. intestinalis*
407 trophozoites was moderately reduced after exposure to nicotinamide. This reduction was similar
408 that found in *Plasmodium*, *Leishmania* and *Trypanosoma* species which have characteristic Sir2
409 (Prusty et al., 2008; Sereno et al., 2005; Soares et al., 2012). Recently, Wang et al. (2016) showed
410 that nicotinamide was able to inhibit activity of GL50803_10707 *Giardia* sirtuin with IC₅₀ value of
411 4.47 mM. As previously demonstrated, *Giardia* sirtuins showed strong homology with SIRT1, and
412 were mostly localized in the nucleus (Carranza et al., 2016; Wang et al., 2016). Since KH-TFMDI
413 has shown activity against SIRT1 in mammalian cell (Huber et al., 2010), it is possible that this
414 compound also inhibit *Giardia* sirtuins. Thus, the effectiveness of KH-TFMDI and nicotinamide in
415 *G. intestinalis* trophozoites indicate that NAD⁺ dependent histone deacetylases could be potential
416 pharmacological targets for giardiasis chemotherapy. It is important to note that KH-TFMDI
417 exposure did not cause cytotoxicity in the Caco-2 cell line. Previous data indicated that KH-TFMDI
418 had promising mammalian cell tolerance indexes when compared to other drugs currently used in
419 clinical therapy for Chagas disease (Veiga-Santos et al., 2014). In accordance with the previously
420 discussed (Veiga-Santos et al., 2014; Verçoza et al., 2017), KH-TFMDI was more selective for the
421 parasite than mammalian cells.

422 The data obtained by light and electron microscopy showed cell rounding upon treatment
423 with KH-TFMDI. This morphological alteration may be accompanied by changes in cytoskeletal
424 elements, since they are associated with cellular stability. It is known that Sir2 proteins have a role
425 in the cytoskeleton dynamics (Hubbert et al., 2002). Recently, Motonishi et al. (2015) reported that
426 SIRT1 would be associated to deacetylating cortactin maintaining actin cytoskeleton integrity in

427 podocytes. SIRT2 protein family, together with HDAC6, has a role in the tubulin deacetylation
428 process regulating the microtubule dynamics in mammalian cells (Hubbert et al., 2002). In *L.*
429 *amazonensis*, the sirtuin inhibitor KH-TFMDI was able to promote a light hyperacetylation of the
430 tubulin that could be related to remodeling of the subpellicular microtubules (Verçoza et al., 2017).
431 Besides that, no change in the tubulin/acetylated tubulin expression or cytoskeleton structures
432 (adhesive disk, median body, *funis*, and axonemes) were observed in *G. intestinalis* trophozoites
433 treated with KH-TFMDI. Interestingly, cell rounding was associated with ventro-lateral flange
434 folding and flagella internalization in trophozoites exposed to this compound. These morphological
435 characteristics are similar to those reported during the first hours of the trophozoite encystation
436 process (Midlej et al., 2008). It is important to mention that in the present study cyst wall protein
437 expression was not observed in the treated culture (Supplementary material 6). Recently, it was
438 demonstrated that treatment of *Giardia* trophozoites with nicotinamide or FR235222, an inhibitor of
439 histone deacetylase (HDAC), blocked cyst wall protein synthesis and hence inhibited encystment
440 (Carranza et al., 2016; Sonda et al., 2010).

441 Concomitant to the effect described above, several changes in the parasite's ultrastructure
442 and process of cell division were noted. The presence of multinucleated and multiflagellated cell
443 masses was seen, suggesting that the cytokinesis could be compromised in trophozoites exposed to
444 this compound. Typical morphological characteristics of cell death seen in other studies (Bagchi et
445 al., 2012; Corrêa et al., 2009), such as membrane blebbing, vacuoles and multi-lamellar bodies were
446 frequently observed. Although *Giardia* is an amitochondrial organism, it presents some autophagic-
447 like and apoptosis-like characteristics (Bagchi et al., 2012; Corrêa et al., 2009). Interestingly,
448 previous works described that inhibition of histone deacetylases or sirtuin function would induce
449 apoptosis in different cellular models (Zhang and Zhong, 2014), including parasites such as *T. cruzi*,
450 *L. infantum* and *L. amazonensis* (Veiga-Santos et al., 2014; Verçoza et al., 2017; Vergnes et al.,
451 2005). To determine if KH-TFMDI would induce cell death in *G. intestinalis* trophozoites, several
452 classical markers were employed in the present study. Annexin V binding was observed in treated

453 trophozoites, indicating that KH-TFMDI treatment could lead to early membrane events in cell
454 death. DNA smear instead of DNA fragmentation, characteristic of apoptotic cell death, was seen in
455 trophozoites after drug exposure. This pattern was observed in other studies of cell death
456 characterization on protozoa, indicating a different mechanism of DNA fragmentation in lower
457 eukaryotes (Chose et al., 2002; Côrrea et al., 2009; Ghosh et al., 2009). The nuclear staining of the
458 treated cells was more intense, possibly associated with apoptotic chromatin condensation. The
459 polymorphic aspect of the nuclei was related to the different sizes of Hoechst-stained structures,
460 possibly indicating an early pyknosis-like process. The previous studies indicated that the activation
461 of apoptosis-like cell death in *G. intestinalis* is different from the classical mechanism, occurring by
462 a pathway independent of caspases (Bagchi et al., 2012; Corrêa et al., 2009). As the entire apoptotic
463 machinery is absent in protozoa, alternative forms of programmed cell death have been considered
464 (Bruchhaus et al., 2007).

465 Taken together, these observations indicate that KH-TFMDI promotes a stress condition that
466 could lead to cell death of trophozoites. Consequently, KH-TFMDI should be considered a
467 promising compound for the treatment of giardiasis due to its effects on protozoan proliferation and
468 ultrastructure, in addition to low toxicity in human cell lines. The present work confirms the histone
469 deacetylation pathway as an important target for the development of new strategies for giardiasis
470 treatment.

472 **Funding**

473 This work was supported by the “Conselho Nacional de Desenvolvimento Científico e
474 Tecnológico” (CNPq), “Financiadora de Estudos e Projetos” (FINEP), and “Fundação Carlos
475 Chagas Filho de Amparo à Pesquisa no Estado do Rio e Janeiro (FAPERJ)”.

476

477 **Acknowledgments**

478 The authors thank Jorge Gomes and Mariana Ribeiro for technical support with DNA
479 analysis. The English language was revised by American Manuscript Editors.

480

481

482

483

484

485

486

487

488

489

490

491

492

493

494

496 **References**

497

498 Abend, A., Kehat, I., 2015. Histone deacetylases as therapeutic targets--from cancer to cardiac
499 disease. *Pharmacol. Ther.* 147, 55-62.

500 Alsford, S., Kawahara, T., Isamah, C., Horn, D., 2007. A sirtuin in the African trypanosome is
501 involved in both DNA repair and telomeric gene silencing but is not required for antigenic
502 variation. *Mol. Microbiol.* 63, 724-736.

503 Argüello-García, R., Cruz-Soto, M., Romero-Montoya, L., Ortega-Pierres, G., 2009. *In vitro*
504 resistance to nitroimidazoles and benzimidazoles in *Giardia duodenalis*: variability and
505 variation in gene expression. *Infect. Genet. Evol.* 9, 1057-1064.

506 Avalos, J.L., Bever, K.M., Wolberger, C., 2005. Mechanism of sirtuin inhibition by nicotinamide:
507 altering the NAD(+) cosubstrate specificity of a Sir2 enzyme. *Mol. Cell.* 17, 855-868.

508 Bagchi, S., Oniku, A.E., Topping, K., Mamhound, Z.N., Paget, T.A., 2012. Programmed cell death
509 in *Giardia*. *Parasitology* 39, 894-903.

510 Bruchhaus, I., Roeder, T., Rennenberg, A., Heussler, V.T., 2007. Protozoan parasites: programmed
511 cell death as a mechanism of parasitism. *Trends Parasitol.* 23, 376-383.

512 Buret, A.G., 2008. Pathophysiology of enteric infections with *Giardia duodenalis*. *Parasite* 15, 261-
513 265.

514 Carranza, P.G., Gargantini, P.R., Prucca, C.G., Torri, A., Saura, A., Svärd, S., Lujan, H.D., 2016.
515 Specific histone modifications play critical roles in the control of encystation and antigenic
516 variation in the early-branching eukaryote *Giardia lamblia*. *Int. J. Biochem. Cell Biol.* 81:32-
517 43.

518 Campanati, L., Gadelha, A.P., Monteiro-Leal, L.H., 2001. Electron and video-light microscopy
519 analysis of the in vitro effects of pyrantel pamoate on *Giardia lamblia*. *Exp. Parasitol.* 97, 9-
520 14.

521 Campanati, L., Monteiro-Leal, L.H., 2002. The effects of the antiprotosoal drugs metronidazole and
522 furazolidone in trophozoites of *Giardia lamblia* (P1 strain). *Parasitol. Res.* 88, 80-85.

523 Carafa, V., Nebbioso, A., Altucci, L., 2012. Sirtuins and disease: the road ahead. *Front. Pharmacol.*
524 31, 3-4.

525 Chose, O., Noel, C., Gerbod, D., Brenner, C., Viscogliosi, E., Roseto, A., 2002. A form of cell
526 death with some features resembling apoptosis in the amitochondrial unicellular organism
527 *Trichomonas vaginalis*. *Exp. Cell Res.* 276, 32–39.

528 Cohen, D.E., Supinski, A.M., Bonkowski, M.S., Donmez, G., Guarente, L.P., 2009. Neuronal
529 SIRT1 regulates endocrine and behavioral responses to calorie restriction. *Genes Dev.* 23,
530 2812-2817.

531 Corrêa, G., Vilela, R., Menna-Barreto, R.F., Midlej, V., Benchimol, M., 2009. Cell death induction
532 in *Giardia lamblia*: effect of beta-lapachone and starvation. *Parasitol. Int.* 58, 424-437.

533 Emery, S.J., Baker, L., Ansell, B.R.E., Mirzaei, M., Haynes, P.A., McConville, M.J., Svärd, S.G.,
534 Jex, A.R., 2018. Differential protein expression and post-translational modifications in
535 metronidazole-resistant *Giardia duodenalis*. *Gigascience* 7, doi: 10.1093/gigascience/giy024.

536 Gardner, T.B., Hill, D.R., 2001. Treatment of Giardiasis. *Clin Microbiol. Rev.* 14, 114-128.

537 Ghosh, E., Ghosh, A., Ghosh, A.N., Nozaki, T., Ganguly, S., 2009. Oxidative stress-induced cell
538 cycle blockage and a protease-independent programmed cell death in microaerophilic *Giardia*
539 *lamblia*. *Drug Des. Dev. Ther.* 3, 103-110.

540 Greiss, S., Gartner, A. 2009. Sirtuin/Sir2 phylogeny, evolutionary considerations and structural
541 conservation. *Mol. Cell* 28, 407-415.

542 Haumaitre, C., Lenoir, O., Scharfmann, R., 2009. Directing cell differentiation with small-molecule
543 histone deacetylase inhibitors: the example of promoting pancreatic endocrine cells. *Cell*
544 *Cycle* 8, 536-544.

545 Horio, Y., Hayashi, T., Kuno, A., Kunitomo, R., 2011. Cellular and molecular effects of sirtuins in
546 health and disease. *Clin. Sci. (Lond)* 121, 191-203.

547 Hubbert, C., Guardiola, A.C., Shao, R., Kawaguchi, Y., Ito, A., Nixon, A., Yoshida, M., Wang,
 548 X.F., Yao, T.P., 2002. HDAC6 is a microtubule-associated deacetylase. *Nature* 417, 455–
 549 458.

550 Huber, K., Schemies, J., Uciechowska, U., Wagner, J.M., Rumpf, T., Lewrick, F., Süß, R., Sippl,
 551 W., Jung, M., Bracher, F., 2010. Novel 3-arylideneindolin-2-ones as inhibitors of NAD⁺-
 552 dependent histone deacetylases (sirtuins). *J. Med. Chem.* 53, 1383-1386.

553 Inoue, T., Hiratsuka, M., Osaki, M., Oshimura, M., 2007. The molecular biology of mammalian
 554 SIRT proteins: SIRT2 in cell cycle regulation. *Cell Cycle* 6, 1011-1018.

555 Karanis, P., Kourenti, C., Smith, H., 2007. Waterborne transmission of protozoan parasites: a
 556 worldwide review of outbreaks and lessons learnt. *J. Water Health* 5, 1-38.

557 Keister, D.B., 1983. Axenic cultivation of *Giardia lamblia* in TYI-S-33 medium supplemented with
 558 bile. *Trans. R. Soc. Trop. Med. Hyg.* 77, 487-488.

559 Kohl, L., Sherwin, T., Gull, K., 1999. Assembly of the paraflagellar rod and the flagellum
 560 attachment zone complex during the *Trypanosoma brucei* cell cycle. *J. Eukaryot. Microbiol.*
 561 46, 105-109.

562 Kouzarides, T., 2007. Chromatin modifications and their function. *Cell* 128, 693-705.

563 MacDonald, L.M., Armson, A., Thompson, A.R. and Reynoldson, J.A. (2004). Characterisation of
 564 benzimidazole binding with recombinant tubulin from *Giardia duodenalis*, *Encephalitozoon*
 565 *intestinalis*, and *Cryptosporidium parvum*. *Mol. Bioch. Parasitol.* 138, 89-96.

566 Margueron, R., Trojer, P., Reinberg, D., 2005. The key to development: interpreting the histone
 567 code? *Curr. Opin. Genet. Dev.* 15, 163-176.

568 Merrick, C.J., Jiang, R.H., Skillman, K.M., Samarakoon, U., Moore, R.M., Dzikowski, R., Ferdig,
 569 M.T., Duraisingh, M.T., 2015. Functional analysis of sirtuin genes in multiple *Plasmodium*
 570 *falciparum* strains. *PLoS One* 10, doi: 10.1371/journal.pone.0118865.

571 Midlej, V., Benchimol, M., 2009. *Giardia lamblia* behavior during encystment: how morphological
 572 changes in shape occur. *Parasitol. Int.* 58, 72-80.

573 Morgan, U.M., Reynoldson, J.A., Thompson, R.C., 1993. Activities of several benzimidazoles and
574 tubulin inhibitors against *Giardia* spp. *in vitro*. *Antimicrob. Agents Chemother.* 37, 328-331.

575 Motonishi, S., Nangaku, M., Wada, T., Ishimoto, Y., Ohse, T., Matsusaka, T., Kubota, N., Shimizu,
576 A., Kadowaki, T., Tobe, K., Inagi, R., 2015. Sirtuin1 maintains actin cytoskeleton by
577 deacetylation of cortactin in injured podocytes. *J. Am. Soc. Nephrol.* 26, 1939-1959.

578 Ong, D.N, Dittrich, S., Swyter, S., Jung, M., Bracher, F., 2017. Synthesis of highly substituted 3-
579 arylideneindolin-2-ones. *Tetrahedron* 73, 5668-5679.

580 Oxberry, M.E., Thompsonm, R.C.A., Reynoldson, J.A., 1994. Evaluation of the effects of
581 albendazole and metronidazole on the ultrastructure of *Giardia duodenalis*, *Trichomonas*
582 *vaginalis* and *Spironucleus muris* using transmission electron microscopy. *Int. J. Parasitol.* 24,
583 695-703.

584 Pérez-Rangel, A., Hernández, J.M., Castillo-Romero, A., Yépez-Mulia, L., Castillo, R., Hernández-
585 Luis, F., Nogueda-Torres, B., Luna-Arias, J.P., Radilla, G., León-Avila, G. 2013. Albendazole
586 and its derivative JVG9 induce encystation on *Giardia intestinalis* trophozoites. *Parasitol.*
587 *Res.* 112, 3251-3257.

588 Prusty, D., Mehra, P., Srivastava, S., Shivange, A.V., Gupta, A., Roy, N., Dhar, S.K., 2008.
589 Nicotinamide inhibits *Plasmodium falciparum* Sir2 activity in vitro and parasite growth.
590 *FEMS Microbiol. Lett.* 282, 266-72.

591 Religa, A.A., Waters, A.P., 2012. Sirtuins of parasitic protozoa: in search of function(s). *Mol.*
592 *Biochem. Parasitol.* 185, 71-88.

593 Ritagliati, C., Alonso, V.L., Manarin, R., Cribb, P., Serra, E.C., 2015. Overexpression of
594 cytoplasmic TcSIR2RP1 and mitochondrial TcSIR2RP3 impacts on *Trypanosoma cruzi*
595 growth and cell invasion. *PLOS Negl. Trop. Dis.* 9, (4):e0003725.

596 Sereno, D., Alegre, A.M., Silvestre, R., Vergnes, B., Ouaisi, A., 2005. *In vitro* antileishmanial
597 activity of nicotinamide. *Antimicrob. Agents Chemother.* 49, 808-812.

598 Soares, M.B., Silva, C.V., Bastos, T.M., Guimarães, E.T., Figueira, C.P., Smirlis, D., Azevedo,
599 W.F. Jr., 2012. Anti-*Trypanosoma cruzi* activity of nicotinamide. *Acta Trop.* 122, 224-229.

600 Sonda, S., Morf, L., Bottova, I., Baetschmann, H., Rehrauer, H., Caflisch, A., Hakimi, M.A., Hehl,
601 A.B., 2010. Epigenetic mechanisms regulate stage differentiation in the minimized protozoan
602 *Giardia lamblia*. *Mol. Microbiol.* 76, 48-67.

603 Tejman-Yarden, N., Eckmann, L., 2011. New approaches to the treatment of giardiasis. *Curr. Opin.*
604 *Infect. Dis.* 24, 451-456.

605 Uzlikova, M., Nohynkova, E., 2014. The effect of metronidazole on the cell cycle and DNA in
606 metronidazole-susceptible and -resistant *Giardia* cell lines. *Mol. Biochem. Parasitol.* 198, 75-
607 81.

608 Veiga-Santos, P., Reignault, L.C., Huber, K., Bracher, F., De Souza, W., De Carvalho, T.M., 2014.
609 Inhibition of NAD⁺-dependent histone deacetylases (sirtuins) causes growth arrest and
610 activates both apoptosis and autophagy in the pathogenic protozoan *Trypanosoma cruzi*.
611 *Parasitology* 141, 814-825.

612 Verçoza, B.R.F., Godinho, J.L.P., de Macedo-Silva, S.T., Huber, K., Bracher, F., de Souza, W.,
613 Rodrigues, J.C.F., 2017. KH-TFMDI, a novel sirtuin inhibitor, alters the cytoskeleton and
614 mitochondrial metabolism promoting cell death in *Leishmania amazonensis*. *Apoptosis* 22,
615 1169-1188.

616 Verdin, E., Hirschey, M.D., Finley, L.W., Haigis, M.C., 2010. Sirtuin regulation of mitochondria:
617 energy production, apoptosis, and signaling. *Trends Biochem. Sci.* 35, 669-675.

618 Vergnes, B., Sereno, D., Tavares, J., Cordeiro-da-Silva, A., Vanhille, L., Madjidian-Sereno, N.,
619 Depoix, D., Monte-Alegre, A., Ouaisi, A., 2005. Targeted disruption of cytosolic SIR2
620 deacetylase discloses its essential role in *Leishmania* survival and proliferation. *Gene* 363, 85-
621 96.

622 Wang, Y.H., Zheng, G.X. and Li, Y.J., 2016. *Giardia duodenalis* Glsir2.2, homolog of SIRT1, is a
623 nuclear-located and AD⁺-dependent deacetylase. *Exp. Parasitol.* 169, 28-33.

- 624 Zemzoumi, K., Sereno, D., François, C., Guilvard, E., Lemesre, J.L., Ouaissi, A., 1998. *Leishmania*
625 *major*: cell type dependent distribution of a 43 kDa antigen related to silent information
626 regulatory-2 protein family. Biol. Cell 90, 239-245.
- 627 Zhang, J., Zhong, Q., 2014. Histone deacetylase inhibitors and cell death. Cell Mol. Life Sci. 71,
628 3885–3890.

630 **Figure Legends**

631

632 **Figure 1.** Growth curves of treated trophozoites for 24 and 48 h. The parasite was cultured in the
633 absence (control) or presence of the KH-TFMDI (a) and metronidazole (b) at the concentration of 1,
634 5, 10 and 25 μ M. The number of parasites in each culture was determined using light microscopy
635 and a hemocytometer, and the results are expressed as the mean \pm SEM (n = 4).

636 **Figure 2.** Live cell images of *G. intestinalis* trophozoites in control and treated culture for 48 h.
637 Untreated parasites exhibited normal morphology, with a pear shape, two nuclei (n) and flagella
638 (arrowhead) (a). Cells treated with 1 μ M of KH-TFMDI exhibited a ruffled aspect (*) of the surface
639 (b). From treatment with 5 μ M KH-TFMDI, cell rounding (c) and formation of asymmetric cell (d)
640 were observed.

641 **Figure 3.** Field emission scanning electron microscopy of *G. intestinalis* trophozoites. Untreated
642 parasites exhibited normal morphology, with a pear shape, four anterior flagella (F), and an
643 adhesive disk (AD) (a). Cells were treated with 1 μ M KH-TFMDI for 48 h (b). Note the membrane
644 blebbing (arrow) on the dorsal surface of the parasite. After treatment with 5 μ M, the cell rounding
645 associated with the ventro-lateral flange folding (small arrow) was observed (c). Note the shrinkage
646 of the body's caudal portion (CR) and a large bulbous structure in the flagellar tip (arrowhead) of
647 some parasites (d). Incomplete cell division and formation of cell masses (e-f) were observed after
648 treatment.

649 **Figure 4.** Immunofluorescence microscopy using TAT-1 (a) and differential interference contrast
650 (DIC) microscopy (a'') of *G. intestinalis* trophozoites. Tubulin was concentrated in the flagella
651 axonemes (arrow), median body (arrowhead), and the whole cell body of trophozoites (a, a'').
652 Hoechst staining was used to label the two oval nuclei (a'). From treatment with 1 μ M KH-TFMDI,
653 some parasites showed a rounded aspect (b, b''). Different sizes of Hoechst-stained structures

654 (arrow) were observed in treated cells (b''). Multinucleated cell masses (*) were seen after treatment
655 with 5 μ M KH-TFMDI (c, c''); an abnormal number of nucleus was also visualized (arrow).

656 **Figure 5.** Automated quantitative fluorescence microscopy of control and treated trophozoites.
657 Example of images collected with the IN Cell imaging system (using a 100 x objective) of control
658 trophozoites. Cells were labeled with Hoechst–nucleus (blue) and anti-tubulin antibody TAT-1 (red)
659 (a). The green line (b) indicates the segmentation of cell area by IN Cell Developer Toolbox 1.9.2.
660 High content analysis of nuclei area (c), nuclei intensity (d), cell area (e) and cell (tubulin) intensity
661 (f), was carried out during trophozoite treatment with different KH-TFMDI concentrations for 48 h.
662 The values are expressed as the mean \pm standard deviation (n = 500 cells).

663 **Figure 6.** Detection of α -tubulin and acetylated α -tubulin in control cells and trophozoites treated
664 with KH-TFMDI by Western blot analysis and densitometry. Each lane was loaded with 35 μ g of
665 protein of whole cell lysates. Immunoblotting using anti- α -tubulin (a) and anti-acetylated α -tubulin
666 antibodies (b). Densitometry analysis of the anti- α -tubulin (c) and anti-acetylated α -tubulin labeling
667 (d). The values plotted in the graphics were normalized using the measurement of the area related to
668 the labeling of the SDS-PAGE gel. The results indicate that there was a slight decreased in the
669 amount of acetylated α -tubulin after treatment with 5 μ M KH-TFMDI, however, this reduction was
670 not significant (n = 3 independent experiments). Immunofluorescence microscopy showed that
671 acetylated tubulin was concentrated in the flagella axonemes, median body (arrows) and adhesive
672 disk (*) of the control (e) and treated trophozoites (f).

673 **Figure 7.** Ultrathin sections of trophozoites observed by transmission electron microscopy. *G.*
674 *intestinalis* (a) showing the nucleus (N), the adhesive disk (arrow), and the typical aspect of the
675 cytoplasm (*) of control parasites (a). Cells treated with KH-TFMDI for 48 h (b-f). Note the
676 abnormal distribution of the cytoplasmic contents (*) after treatment with 1 μ M KH-TFMDI (b).
677 After incubation with 5 μ M KH-TFMDI changes in the cell shape was observed (c), some flagella
678 were internalized in vacuoles (arrowheads in c and inset). Large vacuoles (L) were seen in the

679 cytoplasm of treated cells (e-f).

680 **Figure 8.** Ultrathin sections of *G. intestinalis* treated with KH-TFMDI for 48 h. The nucleus (N)
681 exhibited an abnormal shape profile (a-b) and condensed chromatin (c).

682 **Figure 9.** Quantification of apoptotic parasites by flow cytometry for 48 h. Non-treated parasites
683 (a), cells treated with 1 and 10 μ M KH-TFMDI, respectively (b-c). Left-upper quadrant (R1):
684 positive only for PI; right-upper quadrant (R2): double-positive for annexin V and PI; left-bottom
685 quadrant (R3): no labeling; right-bottom quadrant (R4): positive only for annexin V (b-c). Ten
686 thousand gated events were harvested from each sample. Gel electrophoresis of DNA obtained from
687 the control culture and trophozoites treated with 1 μ M KH-TFMDI (d). Lane 1) 100bp ladder DNA
688 marker; Lane 2) control cells (C); and Lane 3) KH-TFMDI (K1). Observe the sheared fragmented
689 of the trophozoites DNA after treatment with 5 μ M KH-TFMDI (n= 3 independent experiments).

690 **Figure 10.** Analysis of the cell cycle using propidium iodide by flow cytometry. *G. intestinalis*
691 trophozoites were treated with 5 μ M KH-TFMDI for 48 h. The results indicate that there was an
692 increase in the population of cells in G0/G1 and S stage after exposure to KH-TFMDI. The image is
693 representative of 3 independent experiments.

694 **Supplementary material 1.** The chemical structure of the KH-TFMDI inhibitor.

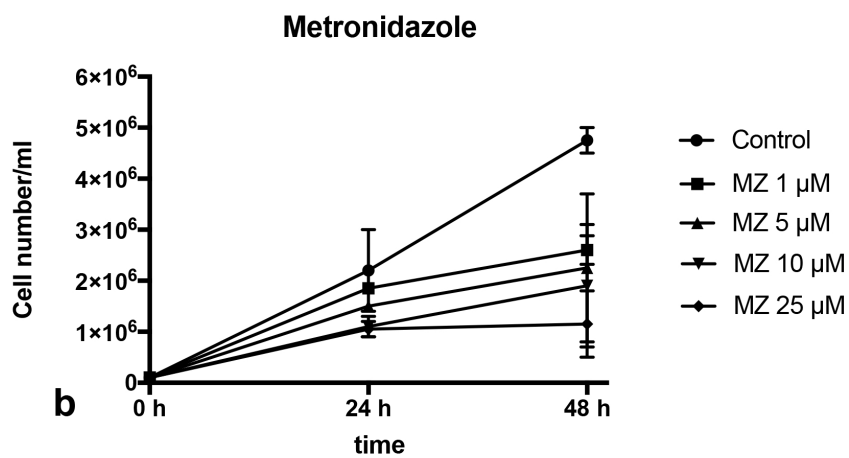
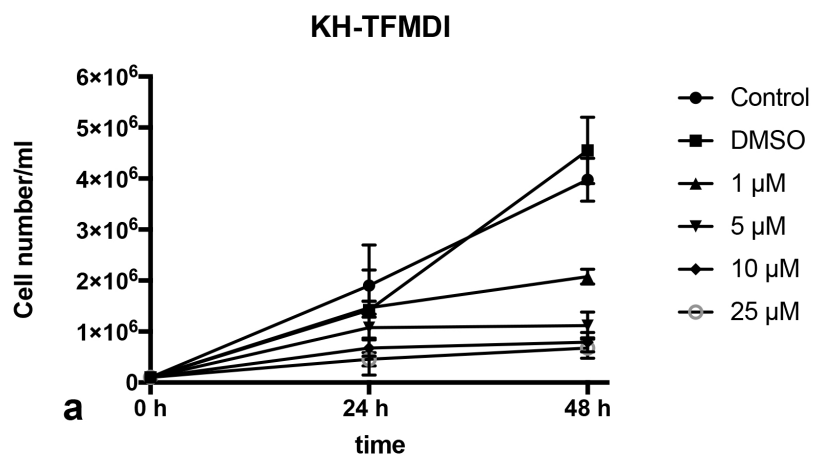
695 **Supplementary material 2.** The amino acid sequence of sirtuin protein aligned to: *Xenopus leavis*
696 (NP_001088636), *Homo sapiens* SIRT1 (NP_036370.2) and SIRT2 (AAK51133.1), *Drosophila*
697 *melanogaster* (AHN57421.1), *Giardia intestinalis* (EET01632), *Trypanosoma grayi*
698 (KEG11227.1), *Leishmania infantum* (AF487351.1), *Entamoeba histolytica* (EHI5A_061340) and
699 *Entamoeba invadens* (EIN_219010). The grey block and arrow show the site of NAD⁺ binding, the
700 black block shows zinc ion binding. The aminoacid sequence are shaded with grey scale, black
701 represent 100% of consensus agreement and white less than 50%.

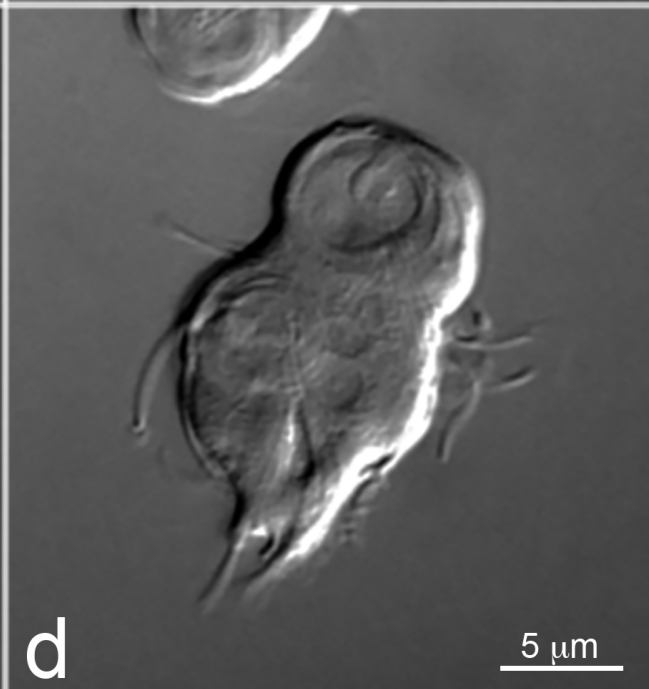
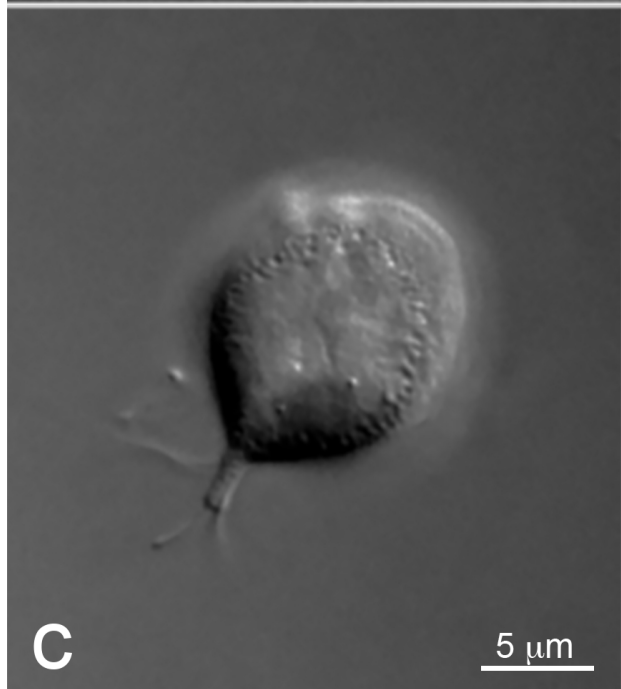
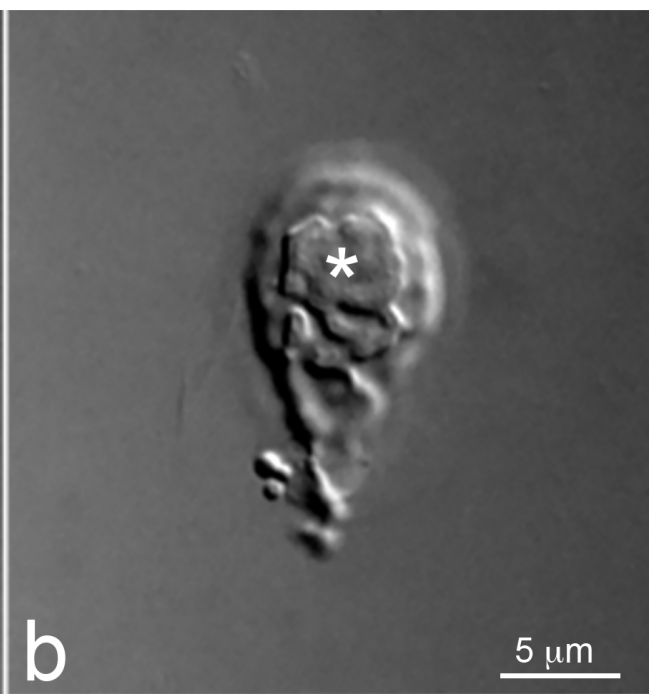
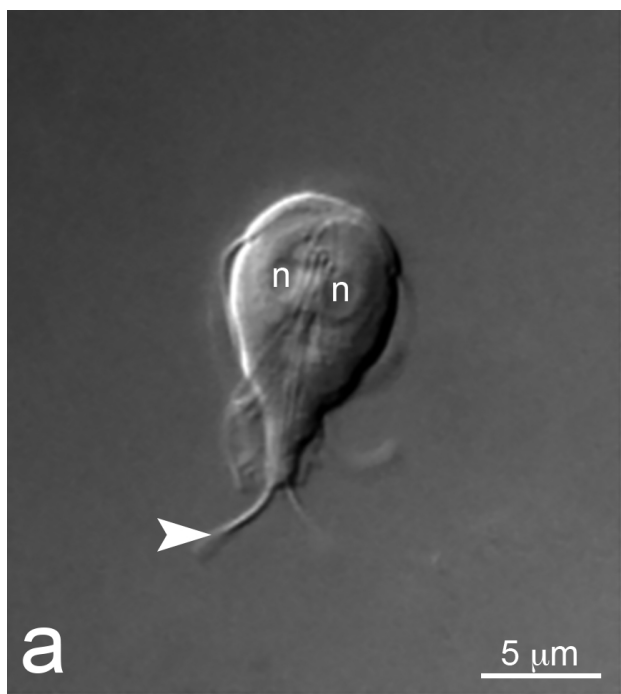
702 **Supplementary material 3.** Growth curve of trophozoites treated with nicotinamide for 24 and 48
703 h. The parasite was cultured in the absence (i.e., the control) or presence of the compound at
704 concentrations of 1, 10, 20 and 50 mM. The number of parasites in each culture was determined
705 using light microscopy and a hemocytometer, and the results are expressed as the mean \pm SEM (n =
706 4).

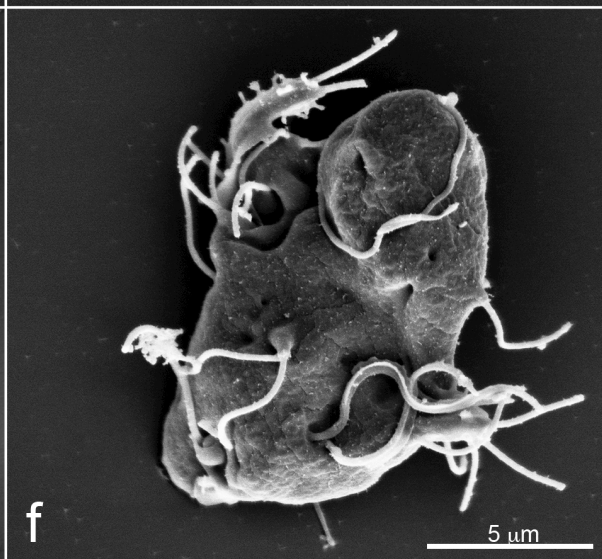
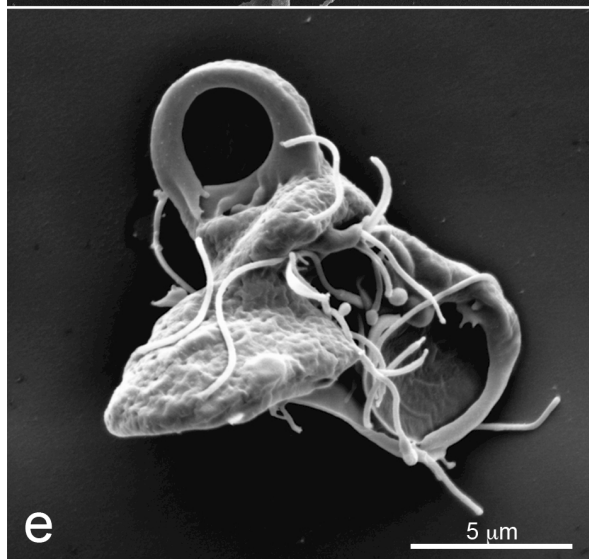
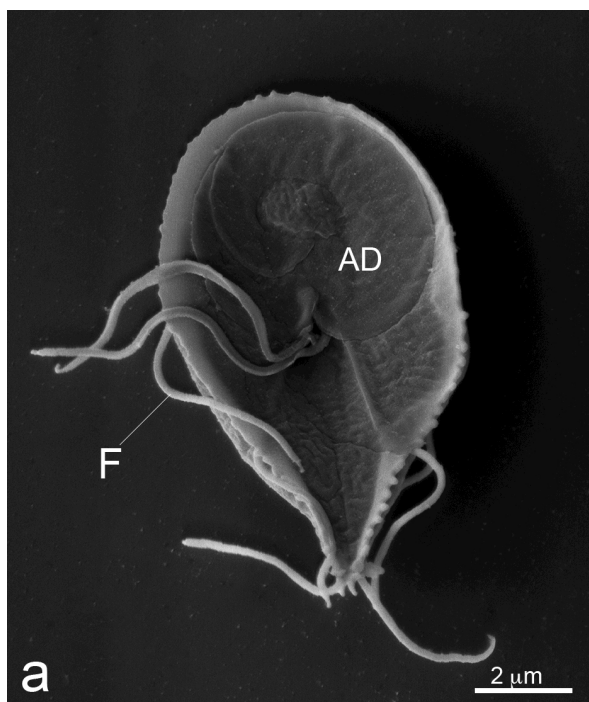
707 **Supplementary material 4.** Automated quantitative fluorescence microscopy of Caco-2
708 proliferation with concentrations of 50 and 100 μ M metronidazole or KH-TFMDI. Caco-2 cells
709 were incubated for 48 h at 37 °C under 5% CO₂. Only fresh DMEM medium containing 10% FBS
710 was added to the untreated samples (i.e., the control). Results are expressed as the mean \pm SEM of
711 two independent experiments, which were each performed in triplicate.

712 **Supplementary material 5.** Immunofluorescence microscopy of cells incubated in the presence of
713 annexin V (green) and propidium iodide (red) in control (a-c) and KH-TFMDI treated (d-f) cultures.
714 It is possible to observe the annexin V labeling on trophozoites exposure to inhibitor (e).

715 **Supplementary material 6.** Immunofluorescence microscopy using Hoechst staining (a) and
716 CWP-specific antibody (b) of *G. intestinalis* trophozoites treated with 5 μ M KH-TFMDI. Cyst wall
717 protein expression was not observed in these cells.



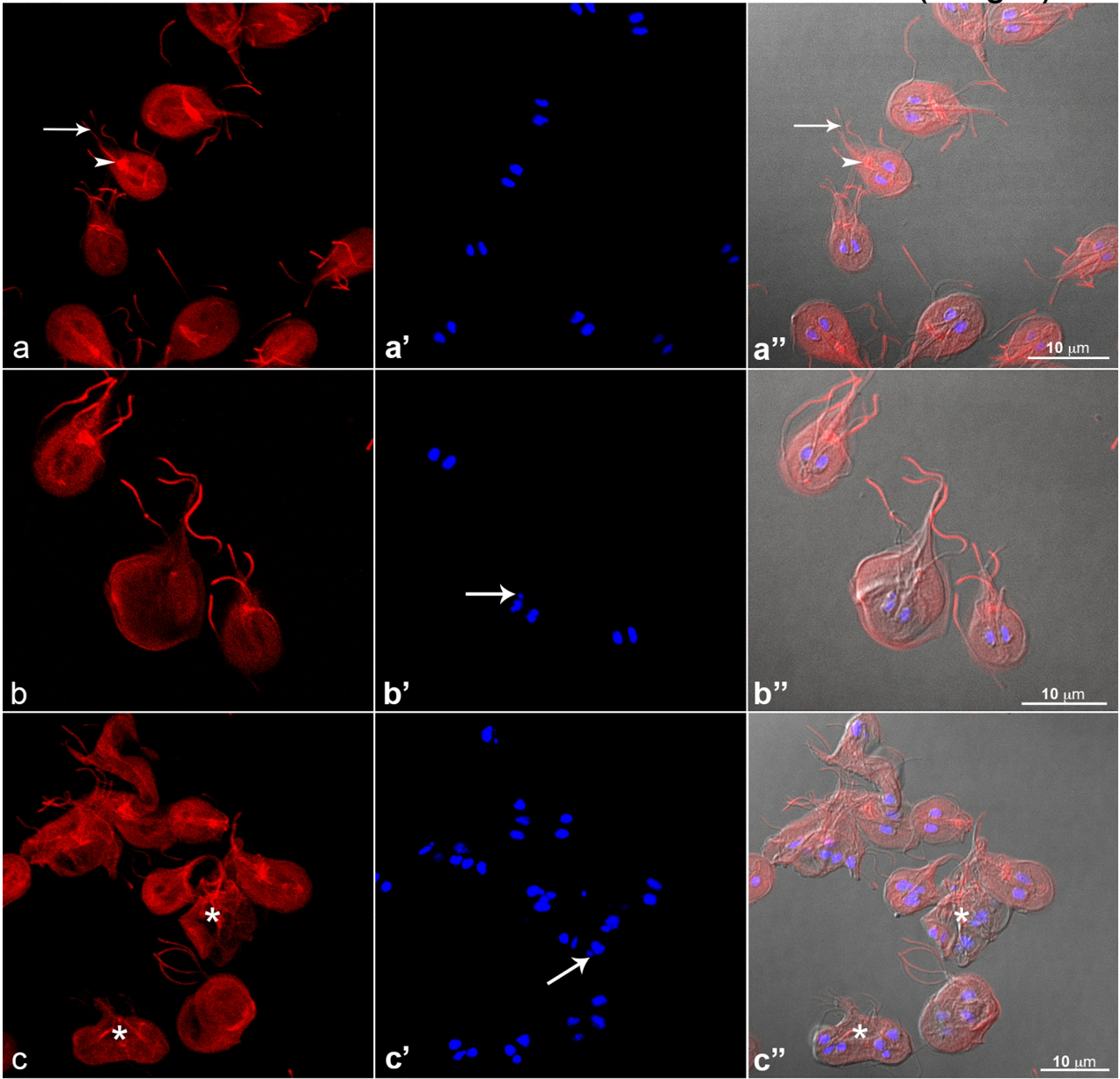


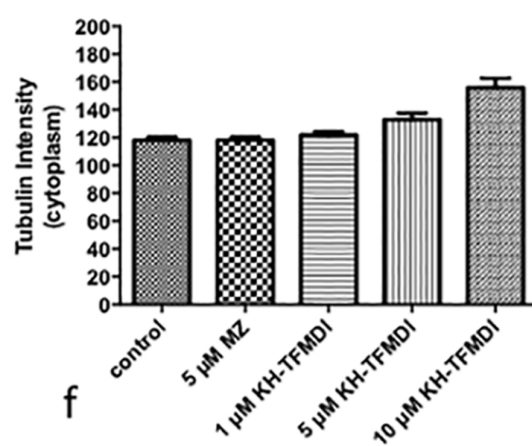
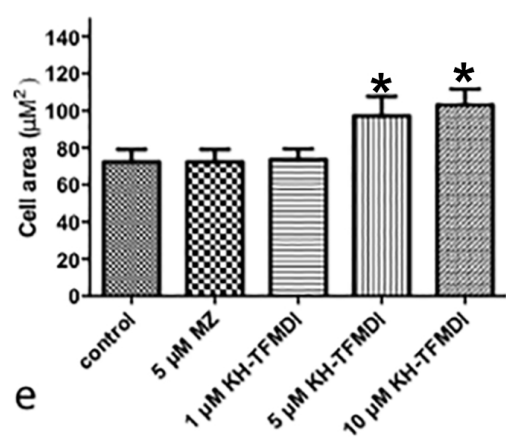
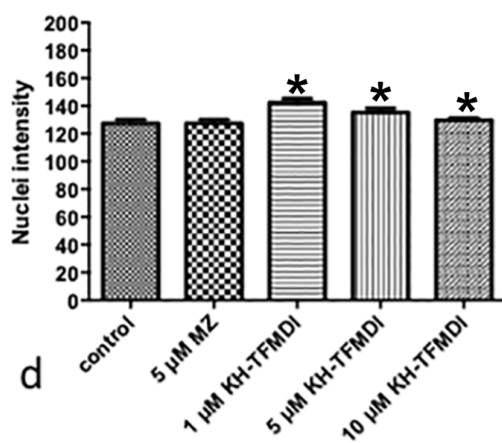
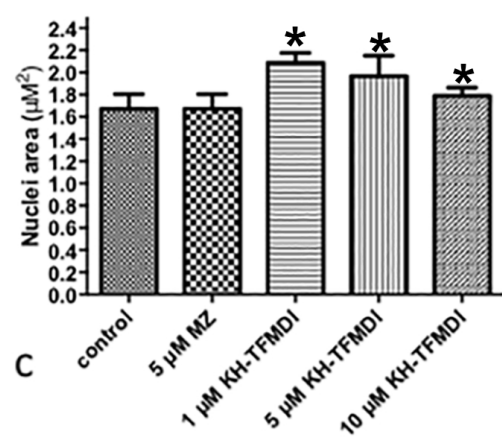
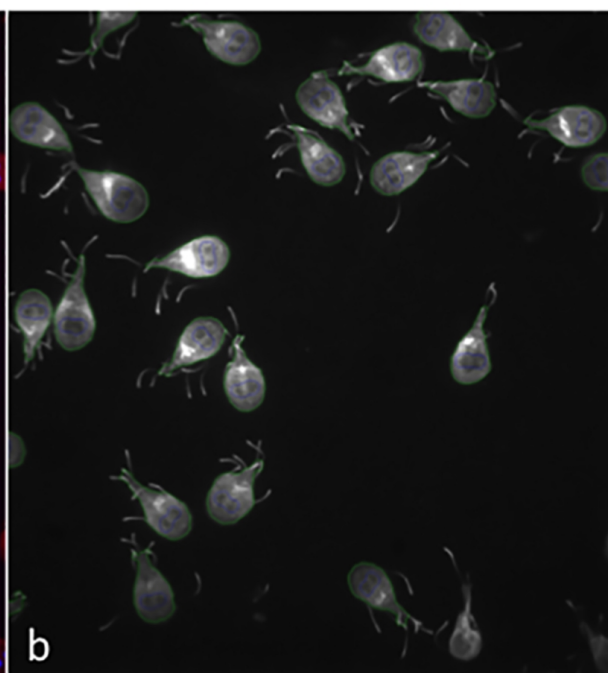
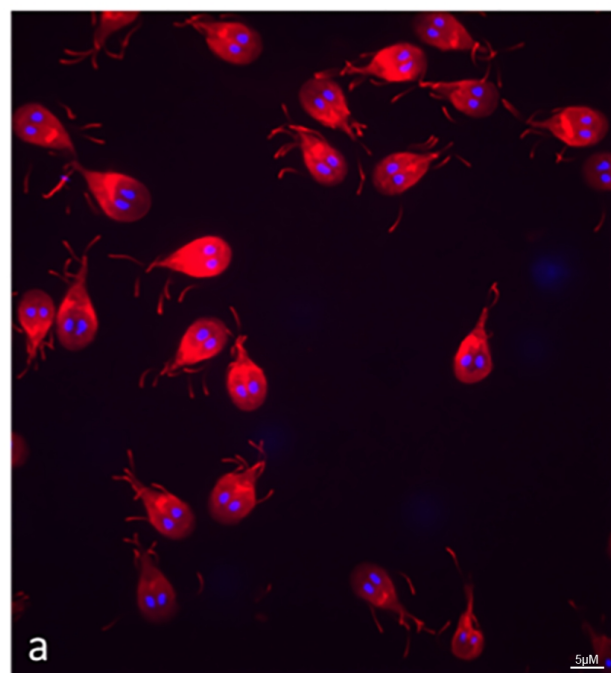


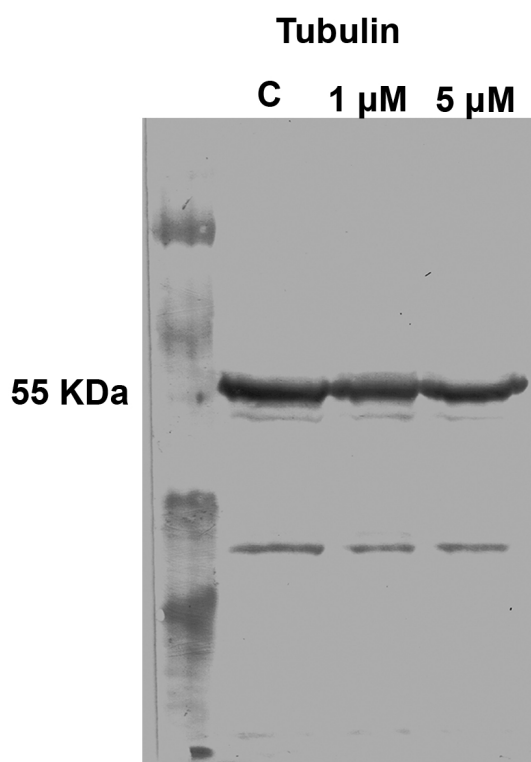
Anti-Tubulin TAT-1

Hoechst

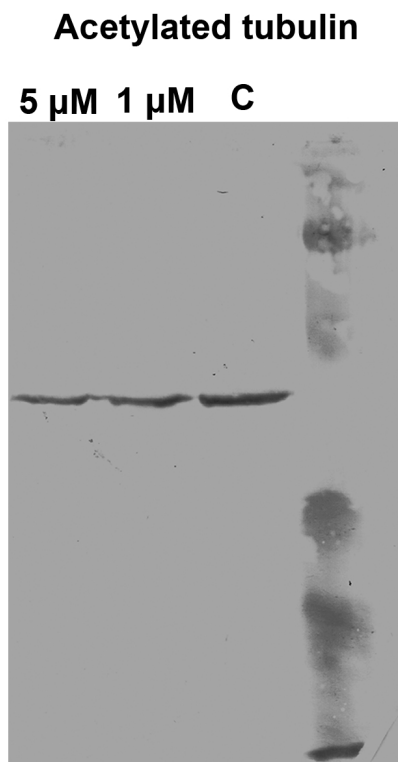
DIC (merged)



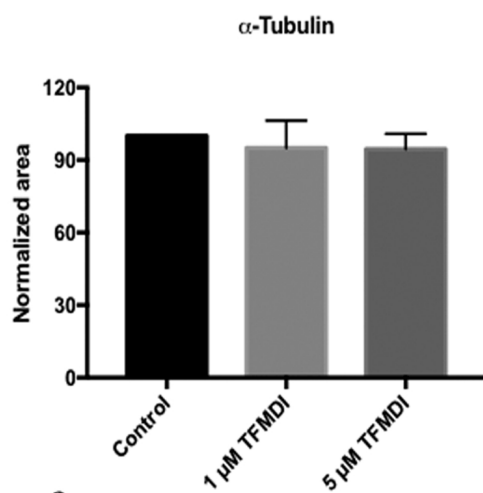




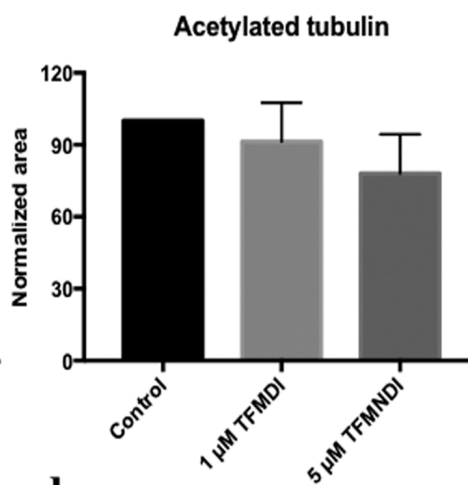
a



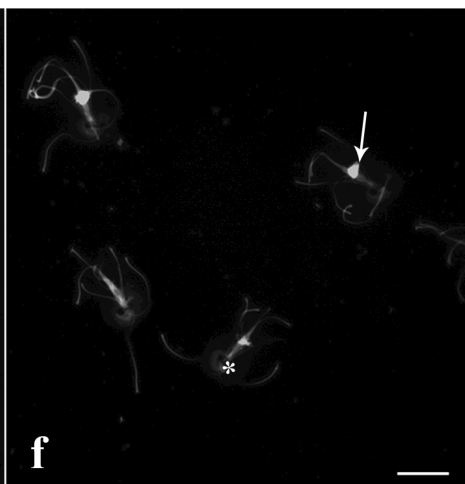
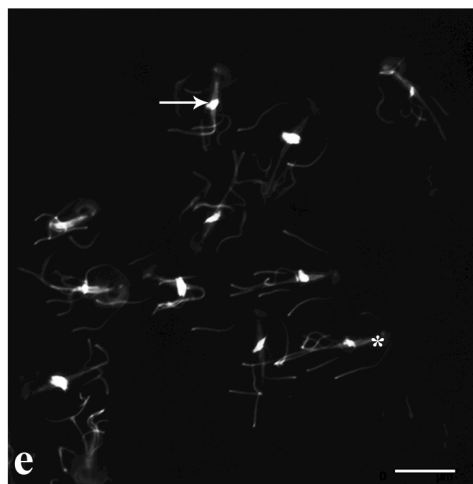
b

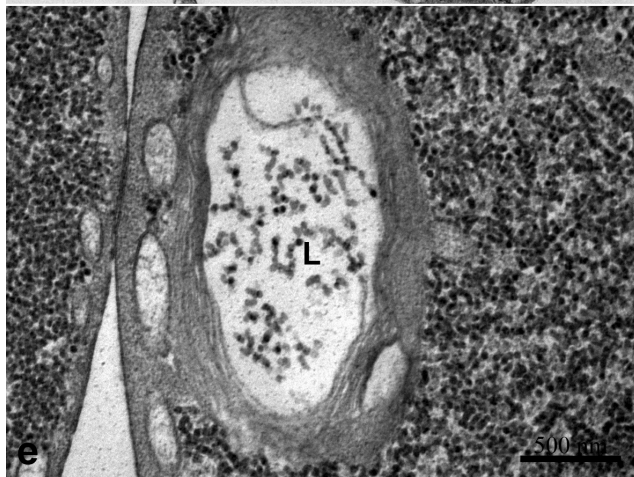
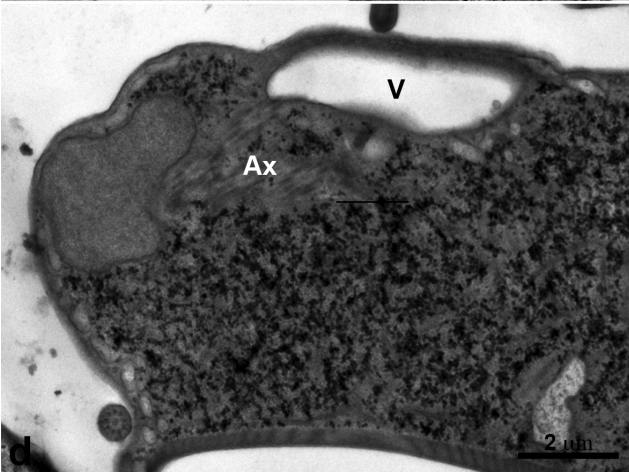
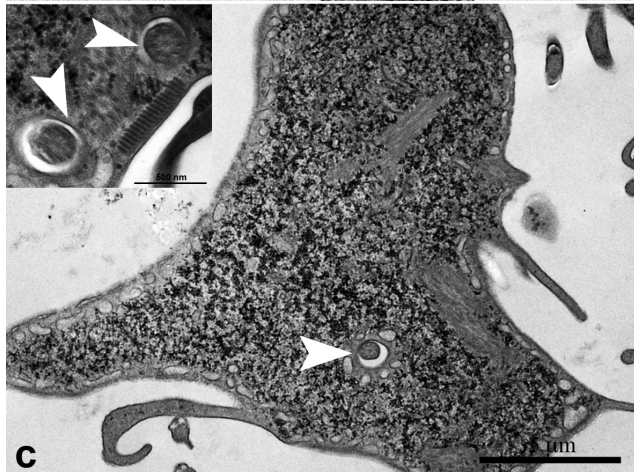
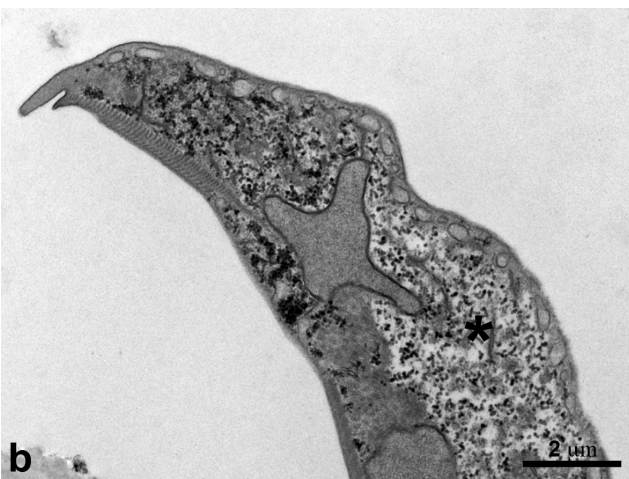
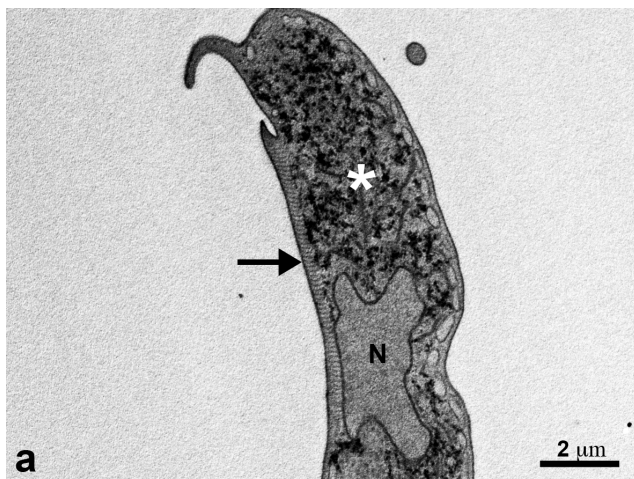


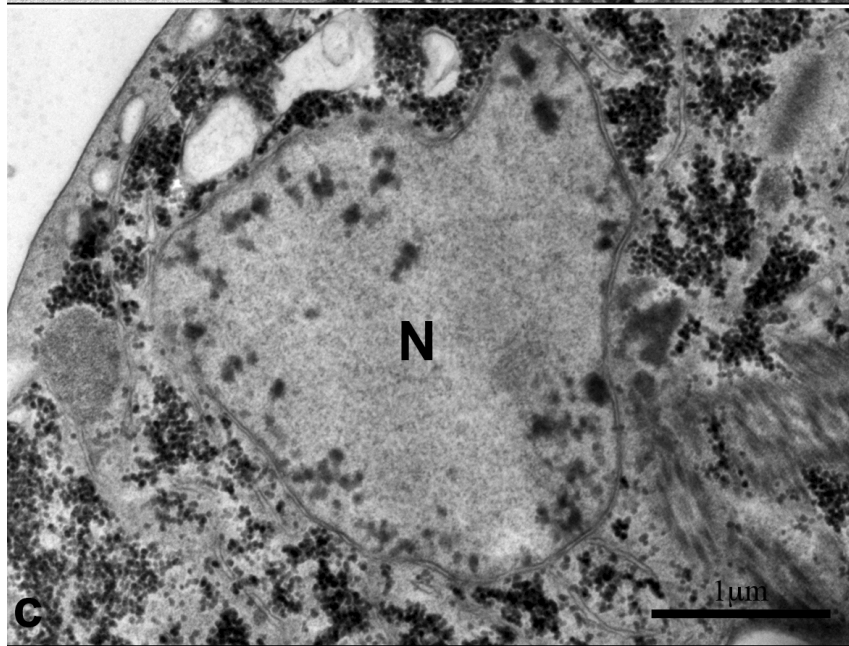
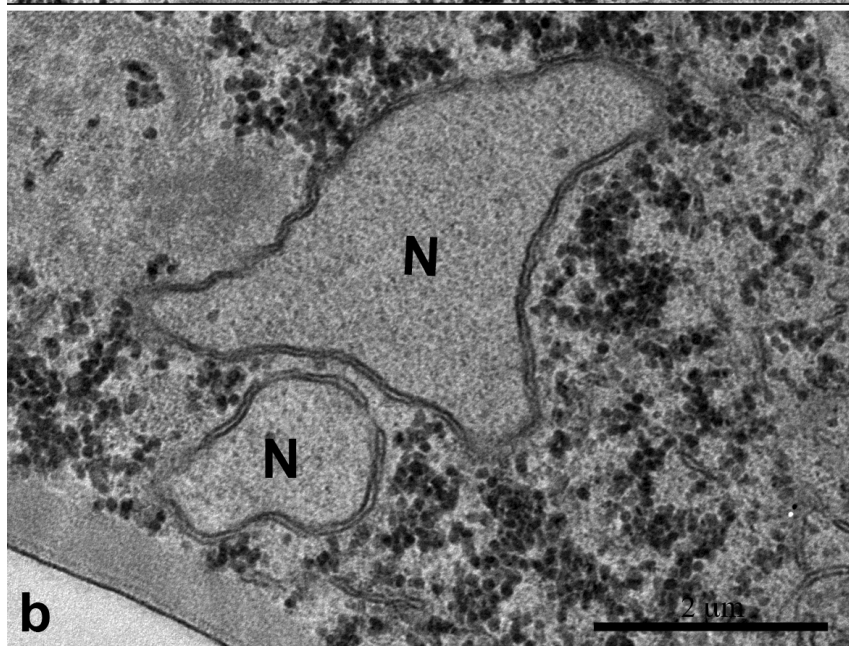
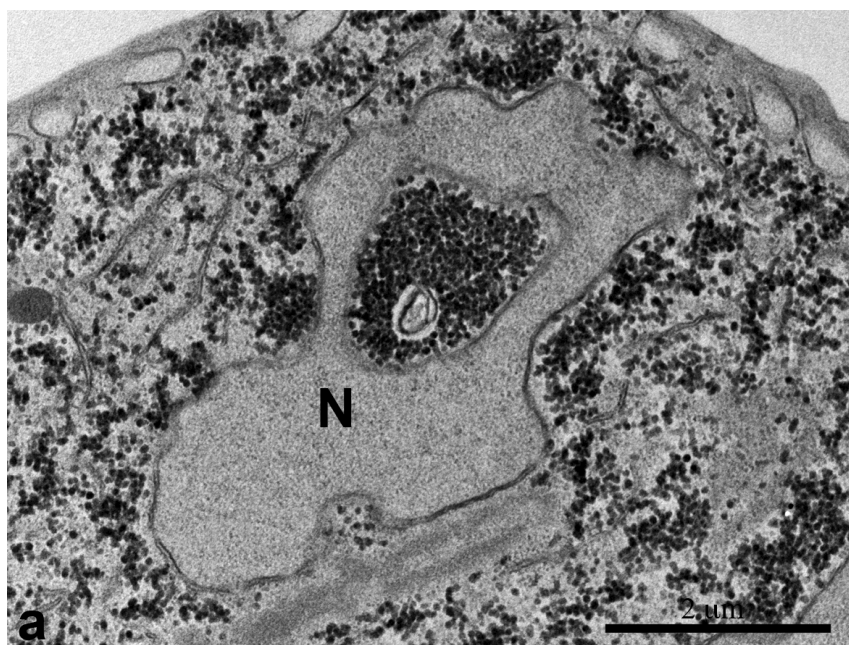
c

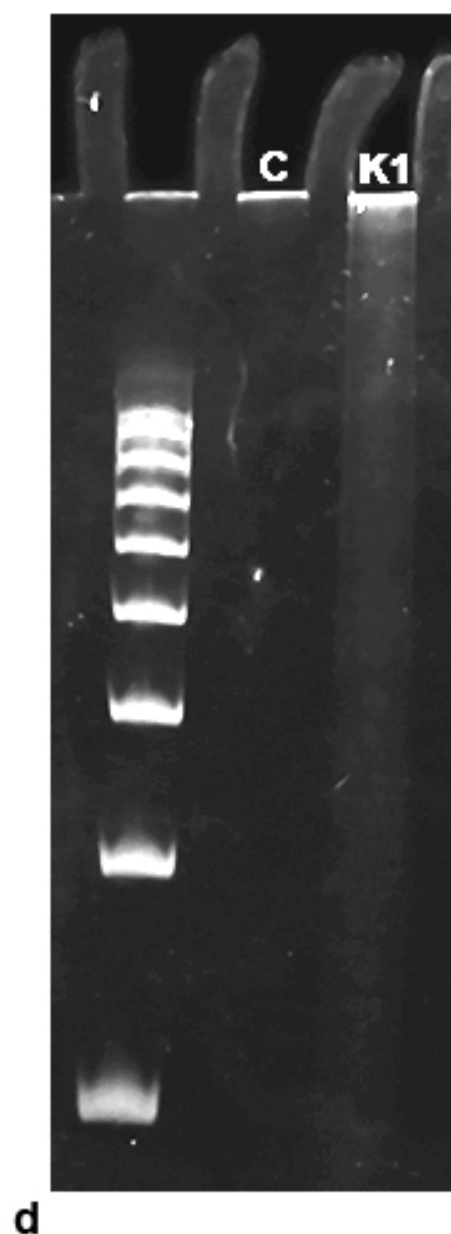
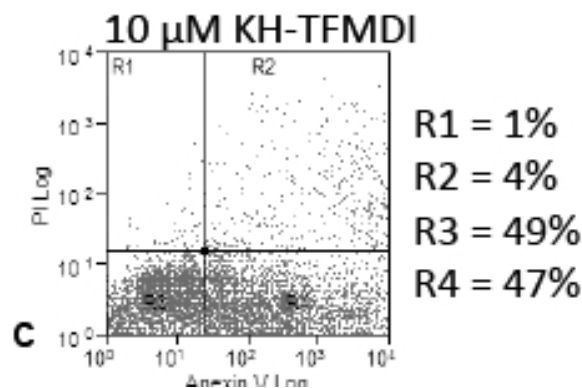
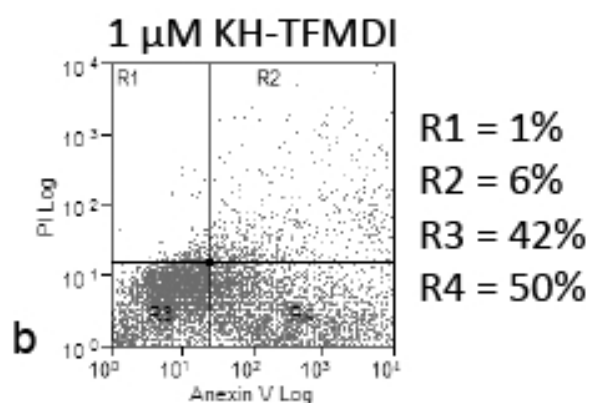
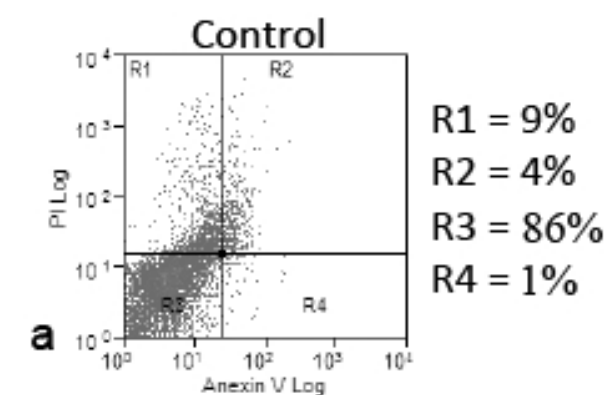


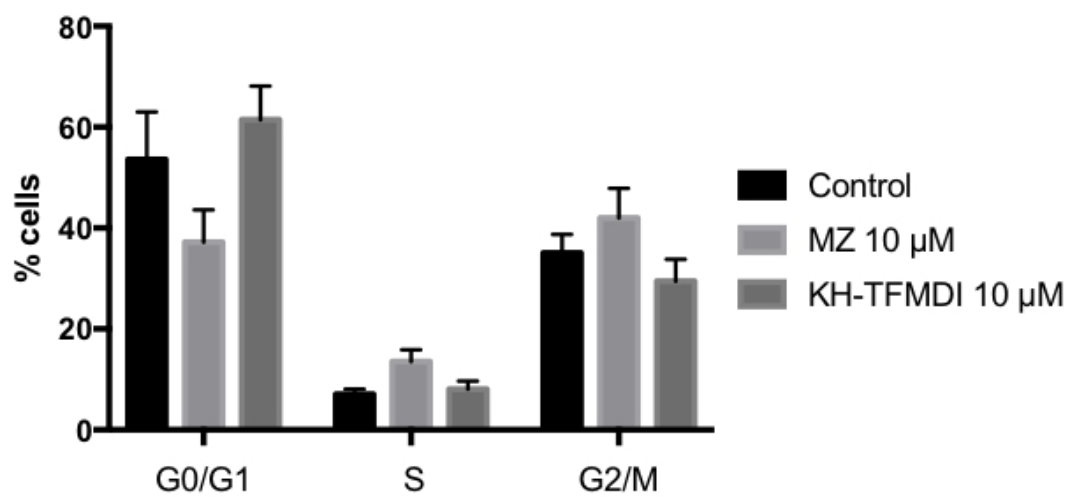
d

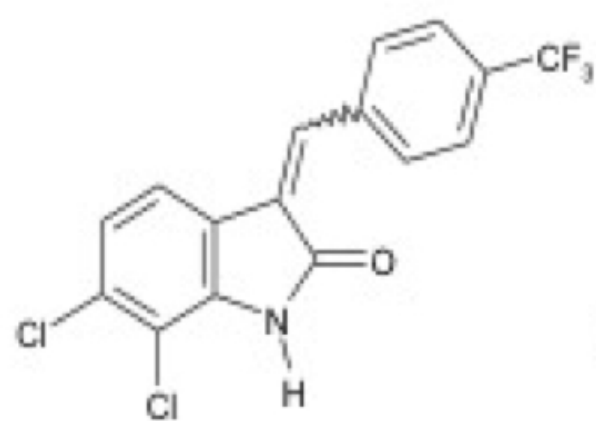












KH-TFMDI

1. *X. leavis*
2. *H. sapiens* (Sirt2)
3. *H. sapiens* (Sirt1)
4. *D. melanogaster*
5. *G. intestinalis*
6. *T. grayi*
7. *L. infantum*
8. *E. histolytica*
9. *E. invadens*

